

## Chemical Equilibration in Hadronic Collisions

Aleksi Kurkela\*

*Theoretical Physics Department, CERN, Geneva, Switzerland and Faculty of Science and Technology,  
University of Stavanger, 4036 Stavanger, Norway*

Aleksas Mazeliauskas†

*Institut für Theoretische Physik, Universität Heidelberg, 69120 Heidelberg, Germany*

 (Received 8 November 2018; revised manuscript received 26 February 2019; published 10 April 2019)

We study chemical equilibration in out-of-equilibrium quark-gluon plasma using the first principles method of QCD effective kinetic theory, accurate at weak coupling. In longitudinally expanding systems—relevant for relativistic nuclear collisions—we find that for realistic couplings chemical equilibration takes place after hydrodynamization, but well before local thermalization. We estimate that hadronic collisions with final state multiplicities  $dN_{\text{ch}}/d\eta \gtrsim 10^2$  live long enough to reach approximate chemical equilibrium, which is consistent with the saturation of strangeness enhancement observed in proton-proton, proton-nucleus, and nucleus-nucleus collisions.

DOI: [10.1103/PhysRevLett.122.142301](https://doi.org/10.1103/PhysRevLett.122.142301)

The experiments at the relativistic heavy ion collider and the large hadron collider (LHC) have seen signs of collective behavior in proton-proton, proton-nucleus, and nucleus-nucleus collisions, which emerge smoothly as a function of the system size measured by event multiplicities. The signals of collectivity include long range multiparticle correlations [1–8], indicative of the onset of flowlike phenomena, and changes in the hadrochemical composition [9–12], indicative of modifications to the process of hadronization in dense medium. The observed enhancement of (multi-)strange hadron yields with respect to pions seems to be fundamentally at odds with the picture of hadronic collisions as independent superpositions of individual partons, and which cannot be reproduced by the tuning of the standard multipurpose event generators [13] without the inclusion of significant new elements [14,15].

In the context of nucleus-nucleus collisions, these observations are understood as signs of kinetically and chemically equilibrated plasma. Fluid dynamic [16–20] and statistical hadronization models [21–24] motivated by local thermal and chemical equilibration of the quark-gluon plasma (QGP) have enjoyed significant phenomenological success over the past decades in describing low momentum hadron production and multiparticle correlations in a range of collision systems. The observed signals of collectivity in

small systems, thus, raise the question whether the picture of locally equilibrated plasma can be extended to small systems, and how this picture eventually breaks down.

How approximately equilibrated plasma emerges from fundamental interactions of the medium constituents has been a topic of intense theoretical study. There have been significant developments in theoretical understanding of far-from-equilibrium dynamics [25,26], kinetic equilibration [27–30], and hydrodynamization [31–35] from first principles. These explorations have however limited themselves to gauge theory models that only resemble QCD, such as pure Yang-Mills theory or  $\mathcal{N} = 4$  supersymmetric Yang-Mills theory, but have not been performed within the full QCD itself, where only near-equilibrium dynamics has been studied [36]. Although for some questions these models can give significant insights, for others—such as chemical equilibration—they lack the essential physics. The fermion production has been previously studied using perturbative estimates of collision rates [37,38], nonperturbative classical-statistical simulations [39,40], solving rate equations [41,42], and pQCD based Boltzmann transport models [43–47]. In this Letter, we address for the first time the emergence of kinetically and chemically equilibrated quark-gluon plasma in full QCD in an *ab initio* framework.

The setup we employ is the effective QCD kinetic theory of Ref. [48], with initial conditions set by saturation framework [49–51]. This systematically improvable setup is accurate in the asymptotic limit of large center-of-mass energies  $\sqrt{s} \rightarrow \infty$ . Although the conditions in physical collisions taking place at relativistic heavy ion collider and the LHC are probably different from this idealized limit, the effective theory framework still provides a semiquantitative

---

*Published by the American Physical Society under the terms of the Creative Commons Attribution 4.0 International license. Further distribution of this work must maintain attribution to the author(s) and the published article's title, journal citation, and DOI. Funded by SCOAP<sup>3</sup>.*

physical picture of QCD dynamics that is strongly rooted in the underlying quantum field theory. The kinetic theory encompasses fluid dynamics in the limit of large number of scatterings, but goes beyond the macroscopic fluid dynamical description and can be used to study systems that are far from equilibrium.

By mapping the only free parameter of the QCD kinetic theory—the coupling constant—to the transport properties in the fluid dynamic limit, we see that the system hydrodynamizes quickly in accordance with findings in pure Yang-Mills theory [28]. We also find that the chemical equilibration takes place after the system has hydrodynamized but before it finally isotropizes. Using the knowledge of the chemical equilibration time, we estimate what is the smallest system that reaches chemical equilibrium and at what multiplicities we expect the hadrochemistry—and therefore also strangeness enhancement—to saturate.

*Setup.*—The kinetic theory that we use to describe equilibration is the effective kinetic theory of Arnold *et al.* [48], which is leading order accurate in the QCD coupling constant  $\lambda = g^2 N_c = 4\pi\alpha_s N_c$ . This framework includes hard thermal loop (HTL) in-medium screening effects [52], and Landau-Pomeranchuk-Migdal [53–56] suppression of collinear radiation in far-from-equilibrium, but parametrically isotropic systems [57]. We extend the previously developed setup of Refs. [27–30] by including quark degrees of freedom [see our companion paper for more details [65]].

We numerically solve the Boltzmann equation for homogeneous boost invariant quark and gluon distribution functions  $f_{g,q}$  according to

$$\partial_\tau f_s(\mathbf{p}, \tau) - \frac{p^z}{\tau} \partial_{p^z} f_s(\mathbf{p}, \tau) = -C_{2 \leftrightarrow 2}^s[f] - C_{1 \leftrightarrow 2}^s[f], \quad (1)$$

where  $\tau$  is the Bjorken time  $\tau = \sqrt{t^2 - z^2}$  [66]. The collision kernel  $C_{2 \leftrightarrow 2}^s[f](\mathbf{p}, \tau)$  is a multidimensional integral over the  $2 \leftrightarrow 2$  scattering matrix elements  $|\mathcal{M}_{cd}^{ab}|^2$  and phase-space factors, which describes the scattering rates for  $gg \leftrightarrow gg$ ,  $gq \leftrightarrow gq$ ,  $qq \leftrightarrow qq$  and  $gg \leftrightarrow q\bar{q}$  processes [48]. For soft small angle scatterings, the tree level scattering matrix  $|\mathcal{M}_{cd}^{ab}|^2$  is divergent and in-medium screening effects must be computed using the HTL resummed propagators. In practice, we supplement the divergent terms appearing in soft gluon or fermion exchanges, e.g.,  $(u-s)/t \sim 1/q^2$ , with an infrared regulator [67]

$$\frac{u-s}{t} \rightarrow \frac{u-s}{t} \frac{q^2}{q^2 + \xi_s^2 m_s^2}, \quad (2)$$

where  $q = |\mathbf{p}' - \mathbf{p}|$  is the momentum transfer in  $t$  channel, and where  $m_{g,q}$  are the in-medium screening masses [48]. Constants  $\xi_g = e^{5/6}/2$  and  $\xi_q = e/2$  are fixed such that the matrix elements reproduce the full HTL results in isotropic systems for drag and momentum diffusion properties of

soft gluon scattering [67] and gluon to quark conversion  $gg \rightarrow q\bar{q}$  [68,69].

The particle number changing processes  $g \leftrightarrow gg$ ,  $q \leftrightarrow qq$ ,  $g \leftrightarrow q\bar{q}$  are included in  $C_{1 \leftrightarrow 2}^s[f](\mathbf{p}, \tau)$  collision kernel [48]. The effective splitting rates are calculated using an isotropic screening approximation [70].

We use color-glass-condensate motivated initial conditions for the gluon distribution function [49,50], which have also been studied in pure gauge theory in [28,30,71,72]. Specifically, at  $\tau_0 = 1/Q_s$ , we take

$$f^g(\mathbf{p}, \tau = \tau_0) = \frac{2A}{\lambda} \frac{Q_0}{\sqrt{p_\perp^2 + p_z^2 \xi^2}} e^{-\frac{2}{3}(p_\perp^2 + \xi^2 p_z^2 / Q_0^2)}, \quad (3)$$

where the values of  $A$  and  $Q_0$ , and  $\xi$  are adjusted to reproduce the typical transverse momentum and energy density from the classical lattice simulations of initial stages of the collision [28,51]. Within the saturation framework, the energy density of fermions is parametrically suppressed compared to that of the gluons and consistently we set the initial fermion energy density to zero in the following. In addition, we have checked that starting with small but nonzero fermion energy density does not change the conclusions.

In collisions with realistic center of mass energies, the QCD coupling constant for in-medium energy scale is not small  $\alpha_s(Q_s \sim 1 \text{ GeV}) \gtrsim 0.3$  [73]. At such values one expects higher order corrections to the macroscopic medium properties. Indeed, next-to-leading order calculations of specific shear viscosity  $\eta/s$  show sizeable modifications of leading order results [74]; however other transport coefficients in units of  $\eta/s$ , e.g.,  $\tau_\pi/[\eta/(sT)]$  are less sensitive to the changes of the coupling constant [75]. Therefore, by adjusting the coupling constant  $\lambda$  to reproduce given specific viscosity  $\eta/s(\lambda)$  [76], we fix the only unspecified parameter of our model and set the overall speed of microscopic dynamics. In practice, we perform simulations for multiple values of  $\lambda$  and map our results to physical values of  $\eta/s$  extracted from other models.

*Results.*—Starting from initial conditions of Eq. (3), we solve the  $N_c = 3$  QCD transport equation Eq. (1) for  $N_f = 3$  flavors of massless fermions. The dynamics of a near-equilibrium system at temperature  $T$  is governed by the kinetic relaxation time, or mean free path

$$\tau_R = \frac{4\pi\eta}{sT} \sim \frac{1}{\lambda^2 T}. \quad (4)$$

At late times when the system is close to local thermal equilibrium, the time evolution of the temperature is given by ideal hydrodynamics with constant  $T(\tau)\tau^{1/3}$ . We follow the practice of [71,72] and find what the temperature of the system would have been at earlier times if the full evolution of the system was described by ideal fluid dynamics

$$T_{\text{id}}(\tau) = \frac{[T(\tau)\tau^{1/3}]|_{\tau \rightarrow \infty}}{\tau^{1/3}}, \quad (5)$$

and define a time dependent kinetic relaxation time  $\tau_R(\tau) = [(4\pi\eta/s)/T_{\text{id}}(\tau)]$ , which we use to compare simulations with different  $\eta/s$ .

The total energy density in a multicomponent plasma is given by a sum of its parts

$$e(\tau) = \int \frac{d^3p}{(2\pi)^3} p^0 (\nu_g f_g + 2N_f \nu_q f_q) = e_g + e_q, \quad (6)$$

where  $\nu_g = 2(N_c^2 - 1)$  and  $\nu_q = 2N_c$ . In chemical equilibrium, the fermion content of the plasma constitutes  $r_q \approx 0.66$  fraction of the total density, i.e.,  $e_{q,\text{eq}} \equiv r_q e$ , where  $r_q^{-1} = 1 + (\nu_g/2N_f\nu_q)^{\frac{8}{3}}$ . We study how the equilibrium fermion energy fraction is reached in Fig. 1 for different values of the coupling constant  $\lambda$ . We see that expressing time in units of kinetic relaxation time  $\tau/\tau_R$  reduces the vast separation of equilibration timescales as shown in the inset plot. For coupling constants  $\lambda = 5, 10, 20$  corresponding to  $\alpha_s \approx 0.1-0.5$ , the chemical equilibration becomes approximately universal. At these moderate couplings, the 90% of fermion equilibrium energy fraction is reached at time  $\tau \approx 1.2\tau_R$ , which we take as our somewhat arbitrary definition of the chemical equilibration time, i.e.,

$$\left| 1 - \frac{e_q(\tau_{\text{chem}})}{e_{q,\text{eq}}} \right| = 0.1, \quad \text{with} \quad \tau_{\text{chem}} = 1.2\tau_R. \quad (7)$$

To quantify the approach to thermal equilibrium and hydrodynamization, we define two additional timescales  $\tau_{\text{therm}}$  and  $\tau_{\text{hydro}}$ , similarly to Eq. (7), by requiring the combined gluon and fermion energy density  $e = e_g + e_q$  to

be within 10% of ideal and viscous hydrodynamic estimates of energy density

$$\left| 1 - \frac{e(\tau_{\text{therm}})}{e_{\text{id}}} \right| = 0.1, \quad \left| 1 - \frac{e(\tau_{\text{hydro}})}{e_{\text{1st}}} \right| = 0.1. \quad (8)$$

Here,  $e_{\text{id}} = (\pi^2/30)(\nu_g + \frac{7}{8}\nu_q 2N_f)T_{\text{id}}^4$  is the ideal estimate of the energy density, and  $e_{\text{1st}} = (\pi^2/30)(\nu_g + \frac{7}{8}\nu_q 2N_f)T_{\text{1st}}^4$ , where  $T_{\text{1st}}$  is the first-order viscous hydrodynamic solution of longitudinally expanding system [77,78]

$$T_{\text{1st}}(\tau) = T_{\text{id}}(\tau) \left( 1 - \frac{2}{12\pi} \frac{\tau_R}{\tau} \right). \quad (9)$$

In Fig. 2, we show the evolution of the total energy density for full QCD kinetic theory (solid red line) for  $\lambda = 10$  ( $\alpha_s \approx 0.26$ ) as a fraction of ideal energy density  $e_{\text{id}}(\tau)$ . We see that the system rapidly approaches hydrodynamic behavior, and at  $\tau_{\text{hydro}} \approx 0.46\tau_R$  the total energy density is within 10% of energy density given by viscous hydrodynamic evolution (black dotted line) [79]. The ideal limit is approached only very slowly, and thermalization takes place at much later times  $\tau_{\text{therm}} \approx 2$ . In the meantime, the chemical composition of plasma undergoes a rapid conversion and the energy density stored in quark degrees of freedom (blue dashed line) quickly overtakes the gluonic component (green dotted line). This results in the following ordering of equilibration timescales

$$\tau_{\text{hydro}} < \tau_{\text{chem}} < \tau_{\text{therm}}, \quad (10)$$

according to the criteria given by Eqs. (7) and (8).

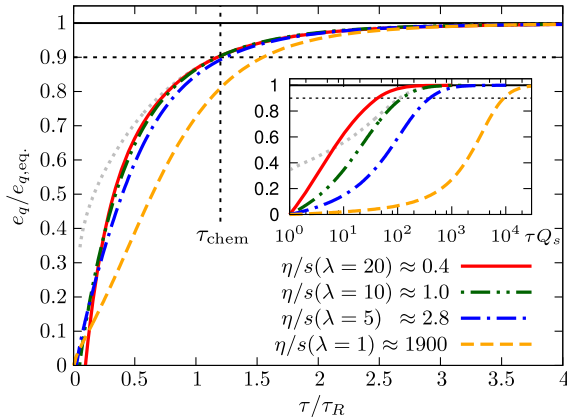


FIG. 1. Fermion energy density fraction of equilibrium density  $e_q(\tau)/e_{q,\text{eq}}(\tau)$  as a function of rescaled time  $\tau/\tau_R = \tau T_{\text{id}}/(4\pi\eta/s)$  for different coupling constants  $\lambda = 1, 5, 10, 20$ . The inset shows unrescaled time dependence on a log-time plot. Gray dotted line shows evolution with nonzero initial fermion density.

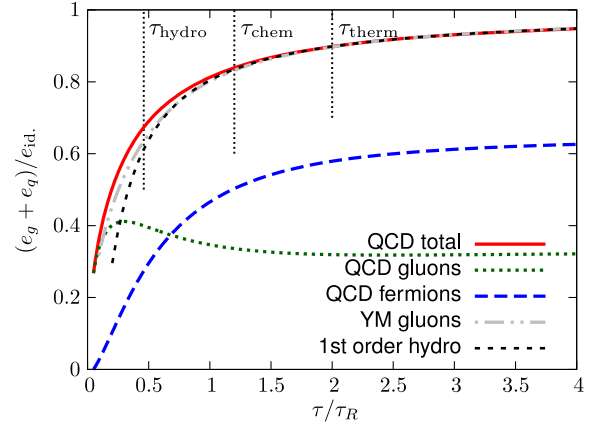


FIG. 2. The total energy density evolution in QCD kinetic theory (red solid line) scaled by ideal asymptotics  $e_{\text{id}} = (\pi^2/30)(\nu_g + \frac{7}{8}\nu_q)T_{\text{id}}^4$  for  $(\eta/s)_{\text{QCD}}(\lambda = 10) \approx 1.0$ . The gluonic and fermionic energy components are shown by green dotted and blue dashed lines correspondingly. In addition, energy evolution in Yang-Mills kinetic theory for the same initial conditions is shown by gray dash-dotted line [ $(\eta/s)_{\text{YM}} \approx 0.62$ ].

We also compare the total energy density evolution in QCD and pure Yang-Mills kinetic theory (gray dashed line) in Fig. 2. After rescaling with corresponding kinetic relaxation time  $\tau_R$  and temperature  $T_{id.}$ , the total energy density evolution is rather similar in both Yang-Mills and QCD kinetic theories. This justifies *a posteriori* the use of pure gauge theory in modeling of the hydrodynamization in nuclear collisions in [71,72]. Finally, we comment in passing that starting with small, but nonzero initial fermion density, does not change the chemical equilibration time as demonstrated by a gray dotted line in Fig. 1 for initial fermion to gluon energy fraction  $e_q/e_g = 0.3$ .

*Discussion.*—As seen in Fig. 1, the process of chemical equilibration becomes insensitive to the value of the coupling constant when measured in properly scaled units. We may use this insensitivity to extrapolate our results to conditions expected to take place in physical collisions at hadron colliders. By taking realistic values of  $(\tau^{1/3}T)|_\infty$  and  $\eta/s$  estimated from hydrodynamical analysis, we convert dimensionless time  $\tau/\tau_R$  into fm/c. This gives us a unique prediction based on first principle QCD kinetic theory for the early time evolution where the fluid dynamical description is not valid. It is a nontrivial question whether such pre-equilibrium evolution will be consistent with the subsequent fluid dynamical evolution of thermally and chemically equilibrated QGP.

Following the procedure presented in [72], the asymptotic constant  $(\tau^{1/3}T)|_\infty$  in kinetic theory can be fixed by the averaged entropy density per rapidity in hydrodynamic simulations

$$(\tau T^3)|_\infty = \langle s\tau \rangle / \left( \frac{4\pi^2}{90} \nu_{\text{eff}} \right), \quad (11)$$

which is a robust quantity and agrees well between different hydrodynamic implementations [30,80,81]. Then  $\tau/\tau_R = \tau T_{id.}/(4\pi\eta/s)$  can be inverted to express physical time in terms of scaled time and asymptotic constants

$$\tau = (\tau/\tau_R)^{3/2} (4\pi\eta/s)^{3/2} \langle s\tau \rangle^{-1/2} \left( \frac{4\pi^2}{90} \nu_{\text{eff}} \right)^{1/2}. \quad (12)$$

We take  $\langle \tau s \rangle \approx 4.1 \text{ GeV}^2$  as a typical value from hydrodynamic simulations for central Pb-Pb collisions at  $\sqrt{s_{NN}} = 2.72 \text{ TeV}$  [30] and  $\nu_{\text{eff}}(0.4 \text{ GeV}) \approx 40$  as the effective number of degrees of freedom obtained from lattice QCD [82,83] (for ideal gas of quarks and gluons  $\nu_{\text{eff}} = 47.5$ ). The specific shear viscosity extracted from comparison of hydrodynamic models and experimental data vary roughly in a range  $\eta/s \approx 0.1\text{--}0.2$  [81,84] and we take  $\eta/s = 2/(4\pi) \approx 0.16$ , which was also used in Ref. [72].

In Fig. 3, we show the energy evolution of Fig. 2 now converted to physical units according to Eq. (12). We see

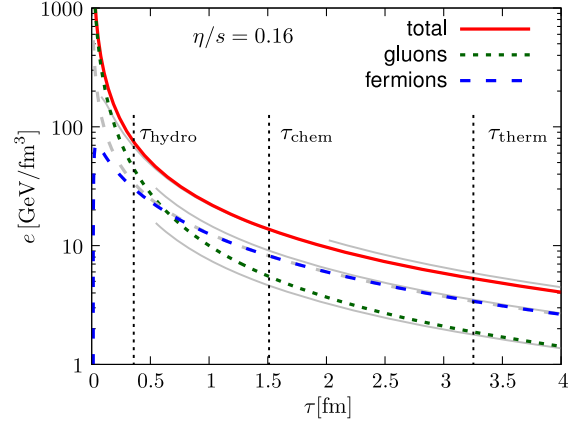


FIG. 3. Evolution of total energy density and its gluonic and fermion components in kinetic theory converted to physical units using universality of  $\tau/\tau_R$  scaling and physical values of  $\eta/s = 0.16$ ,  $\langle s\tau \rangle = 4.1 \text{ GeV}^2$ , and  $\nu_{\text{eff}} = 40$ . The gray solid lines correspond to ideal, viscous, and chemically equilibrated energies. Gray dashed line corresponds to fermion energy evolution with nonzero initial fermion density. The time axis dependence on asymptotic constants is given by  $\tau[\text{fm}] \times (\eta/s/0.16)^{3/2} (\langle s\tau \rangle / 4.1 \text{ GeV}^2)^{-1/2} (\nu_{\text{eff}}/40)^{1/2}$ , whereas the energy axis scales as  $e[\text{GeV}/\text{fm}^3] \times (\eta/s/0.16)^{-2} (\langle s\tau \rangle / 4.1 \text{ GeV}^2)^2 (\nu_{\text{eff}}/40)^{-1}$ .

that starting with initial conditions with no fermions, the fermion energy density increases rapidly to its maximum value at very early times. When this maximum is reached depends sensitively on the initial conditions of the fermions, and for nonzero initial fermion distribution the energy density can even decrease monotonically (gray dashed line). Although this uncertainty does not affect the equilibration times, there are observables, such as photon or dilepton production, that may be sensitive to the initial fermion fraction at early times. At later times, the fermionic energy density decreases slower than the gluonic component, thus increasing the fermion fraction. At times  $\tau \sim 0.7 \text{ fm}$  fermion energy density starts to dominate and  $\tau \sim 1.5 \text{ fm}$  fermionic energy fraction is within 10% of equilibrium value shown by gray line. Finally, if the system continues expanding with boost and transverse translation invariance, then at  $\tau \sim 3.3 \text{ fm}$  energy density evolution is within 10% of the ideal hydrodynamic expectation and the system can be considered locally thermalized.

However, the approximation of transverse translational invariance breaks when the central parts of the collision come into causal contact with the edge of the fireball and the system starts to undergo significant radial expansion. Following the logic of Ref. [72], we assume that the system disintegrates once its lifetime exceeds  $\tau \sim R$  and a three-dimensional expansion begins, where  $R$  is the initial transverse radius of the system [85]. The charged particle multiplicity  $dN_{\text{ch}}/d\eta$  in the final state can be related to the entropy density according to  $\langle \tau s \rangle \approx (S/N_{\text{ch}}) 1/A_\perp dN_{\text{ch}}/d\eta$ , where  $A_\perp \approx \pi R^2$  and  $S/N_{\text{ch}} \approx 7$  are a constant of hadron gas [87,88]. We can

now ask what is the minimal system multiplicity that can achieve chemical equilibration before freezing out. Rewriting Eq. (12) as a bound on multiplicities, we get

$$\frac{dN_{\text{ch}}}{d\eta} \gtrsim 110 \left( \frac{\tau_{\text{chem}}}{1.2\tau_R} \right)^3 \left( \frac{\eta/s}{0.16} \right)^3 \left( \frac{\tau_{\text{chem}}}{R} \right)^{-2}, \quad (13)$$

where other constants were set to their nominal values [89]. That is, using the equilibration rates of QCD kinetic theory, we estimate that chemically equilibrated QGP with specific shear-viscosity  $\eta/s = 0.16$  can be formed only for systems with multiplicity  $dN_{\text{ch}}/d\eta \gtrsim 10^2$  by the time it starts to freeze out at  $\tau \sim R$ .

Experimental measurements of strangeness enhancement in p-p, p-Pb, and Pb-Pb collisions clearly indicate a continuous increase of strangeness production, which is saturated around  $dN_{\text{ch}}/d\eta \sim 10^2$  [11,12]. Our calculation does not contain the necessary ingredients to describe the hadrochemistry in detail [90]. However, assuming that the underlying physics that saturates the strangeness production is the formation of chemically equilibrated plasma, our chemical equilibration rate gives a necessary condition for the event multiplicities where the saturation can take place. We note that as Eq. (13) does not depend on the physical size of the system other than in the combination  $\tau_{\text{chem}}/R \sim 1$ , our calculation is consistent with the observed overlap of strangeness enhancement across different collision systems, when plotted as a function of multiplicity. For  $\eta/s = 0.16$ , our estimate of the multiplicity where we expect strangeness saturation to take place roughly agrees with the experimental observation. Although our estimate is strongly dependent on the definition of  $\tau_{\text{chem}}$  and the assumption that the process of equilibration terminates at  $\tau_{\text{chem}}/R \sim 1$ , it still seems that large values of  $\eta/s \sim 1$  would be in contradiction with chemically equilibrated QGP for  $dN_{\text{ch}}/d\eta \sim 10^2$  thanks to the strong dependence on specific shear viscosity in Eq. (13). In conclusion, in this novel way, we connect the dynamical transport properties of quark-gluon plasma to hadrochemical output. Equation (13) predicts that the saturation of strangeness enhancement should be observed at the same final state multiplicity across different collision systems. We expect that the future high-luminosity studies of proton-proton, proton-nucleus, and nucleus-nucleus collisions at the LHC will answer this question conclusively [94].

Authors would like to thank Peter Arnold, Jürgen Berges, Ulrich Heinz, Jacopo Ghiglieri, Jean-François Paquet, Sören Schlichting, Derek Teaney, and Urs Wiedemann for valuable discussions. This work was supported in part by the German Research Foundation (DFG) Collaborative Research Centre (SFB) 1225 (ISOQUANT) (A. M.). Finally, A. M. would like to thank CERN Theoretical Physics Department for the hospitality during the short-term visit.

\*a.k@cern.ch

†a.mazeliauskas@thphys.uni-heidelberg.de

- [1] B. B. Abelev *et al.* (ALICE Collaboration), Multiparticle azimuthal correlations in p-Pb and Pb-Pb collisions at the CERN Large Hadron Collider, *Phys. Rev. C* **90**, 054901 (2014).
- [2] M. Aaboud *et al.* (ATLAS Collaboration), Correlated long-range mixed-harmonic fluctuations measured in  $pp$ ,  $p + \text{Pb}$  and low-multiplicity  $\text{Pb} + \text{Pb}$  collisions with the ATLAS detector, *Phys. Lett. B* **789**, 444 (2019).
- [3] M. Aaboud *et al.* (ATLAS Collaboration), Measurement of long-range multiparticle azimuthal correlations with the subevent cumulant method in  $pp$  and  $p + \text{Pb}$  collisions with the ATLAS detector at the CERN large hadron collider, *Phys. Rev. C* **97**, 024904 (2018).
- [4] A. M. Sirunyan *et al.* (CMS Collaboration), Observation of Correlated Azimuthal Anisotropy Fourier Harmonics in  $pp$  and  $p + \text{Pb}$  Collisions at the LHC, *Phys. Rev. Lett.* **120**, 092301 (2018).
- [5] C. Aidala *et al.* (PHENIX Collaboration), Creating small circular, elliptical, and triangular droplets of quark-gluon plasma, *Nat. Phys.* **15**, 214 (2019).
- [6] A. Adare *et al.* (PHENIX Collaboration), Multi-particle azimuthal correlations for extracting event-by-event elliptic and triangular flow in Au+Au collisions at  $\sqrt{s_{NN}} = 200$  GeV, *Phys. Rev. C* **99**, 024903 (2019).
- [7] J. Adams *et al.* (STAR Collaboration), Azimuthal anisotropy in Au+Au collisions at  $\sqrt{s_{NN}} = 200$  GeV (1/2) = 200-GeV, *Phys. Rev. C* **72**, 014904 (2005).
- [8] L. Adamczyk *et al.* (STAR Collaboration), Beam Energy Dependence of the Third Harmonic of Azimuthal Correlations in Au + Au Collisions at RHIC, *Phys. Rev. Lett.* **116**, 112302 (2016).
- [9] B. I. Abelev *et al.* (STAR Collaboration), Enhanced strange baryon production in Au + Au collisions compared to  $p + p$  at  $\sqrt{s_{NN}} = 200$  GeV, *Phys. Rev. C* **77**, 044908 (2008).
- [10] B. B. Abelev *et al.* (ALICE Collaboration), Multi-strange baryon production at mid-rapidity in Pb-Pb collisions at  $\sqrt{s_{NN}} = 2.76$  TeV, *Phys. Lett. B* **728**, 216 (2014); Erratum, *Phys. Lett. B* **734**, 314 (2014).
- [11] B. B. Abelev *et al.* (ALICE Collaboration), Multiplicity dependence of pion, kaon, proton and lambda production in p-Pb collisions at  $\sqrt{s_{NN}} = 5.02$  TeV, *Phys. Lett. B* **728**, 25 (2014).
- [12] J. Adam *et al.* (ALICE Collaboration), Enhanced production of multi-strange hadrons in high-multiplicity proton-proton collisions, *Nat. Phys.* **13**, 535 (2017).
- [13] A. Buckley *et al.*, General-purpose event generators for LHC physics, *Phys. Rep.* **504**, 145 (2011).
- [14] N. Fischer and T. Sjöstrand, Thermodynamical string fragmentation, *J. High Energy Phys.* **01** (2017) 140.
- [15] T. Sjöstrand, Collective effects: The viewpoint of HEP MC codes, in *Proceedings of 27th International Conference on Ultrarelativistic Nucleus-Nucleus Collisions (Quark Matter 2018)* (Venice, Italy, 2018).
- [16] U. Heinz and R. Snellings, Collective flow and viscosity in relativistic heavy-ion collisions, *Annu. Rev. Nucl. Part. Sci.* **63**, 123 (2013).

- [17] D. A. Teaney, Viscous hydrodynamics and the quark gluon plasma, in *Quark-Gluon Plasma 4*, edited by R. C. Hwa and X.-N. Wang (World Scientific Publishing Co., Singapore, 2010), pp. 207–266.
- [18] M. Luzum and H. Petersen, Initial state fluctuations and final state correlations in relativistic heavy-ion collisions, *J. Phys. G* **41**, 063102 (2014).
- [19] C. Gale, S. Jeon, and B. Schenke, Hydrodynamic modeling of heavy-ion collisions, *Int. J. Mod. Phys. A* **28**, 1340011 (2013).
- [20] R. Derradi de Souza, T. Koide, and T. Kodama, Hydrodynamic approaches in relativistic heavy ion reactions, *Prog. Part. Nucl. Phys.* **86**, 35 (2016).
- [21] P. Braun-Munzinger, K. Redlich, and J. Stachel, Particle production in heavy ion collisions, *Quark-Gluon Plasma* **3**, 491 (2004).
- [22] J. Cleymans, I. Kraus, H. Oeschler, K. Redlich, and S. Wheaton, Statistical model predictions for particle ratios at  $s(NN)^{1/2} = 5.5$ -TeV, *Phys. Rev. C* **74**, 034903 (2006).
- [23] A. Andronic, P. Braun-Munzinger, and J. Stachel, Thermal hadron production in relativistic nuclear collisions: The Hadron mass spectrum, the horn, and the QCD phase transition, *Phys. Lett. B* **673**, 142 (2009); Erratum, *Phys. Lett. B* **678**, 516 (2009).
- [24] A. Andronic, P. Braun-Munzinger, K. Redlich, and J. Stachel, Decoding the phase structure of QCD via particle production at high energy, *Nature (London)* **561**, 321 (2018).
- [25] J. Berges, K. Boguslavski, S. Schlichting, and R. Venugopalan, Universal attractor in a highly occupied non-Abelian plasma, *Phys. Rev. D* **89**, 114007 (2014).
- [26] J. Berges, K. Boguslavski, S. Schlichting, and R. Venugopalan, Turbulent thermalization process in heavy-ion collisions at ultrarelativistic energies, *Phys. Rev. D* **89**, 074011 (2014).
- [27] A. Kurkela and E. Lu, Approach to Equilibrium in Weakly Coupled Non-Abelian Plasmas, *Phys. Rev. Lett.* **113**, 182301 (2014).
- [28] A. Kurkela and Y. Zhu, Isotropization and Hydrodynamization in Weakly Coupled Heavy-Ion Collisions, *Phys. Rev. Lett.* **115**, 182301 (2015).
- [29] L. Keegan, A. Kurkela, P. Romatschke, W. van der Schee, and Y. Zhu, Weak and strong coupling equilibration in nonabelian gauge theories, *J. High Energy Phys.* **04** (2016) 031.
- [30] L. Keegan, A. Kurkela, A. Mazeliauskas, and D. Teaney, Initial conditions for hydrodynamics from weakly coupled pre-equilibrium evolution, *J. High Energy Phys.* **08** (2016) 171.
- [31] M. P. Heller and M. Spalinski, Hydrodynamics Beyond the Gradient Expansion: Resurgence and Resummation, *Phys. Rev. Lett.* **115**, 072501 (2015).
- [32] M. P. Heller, A. Kurkela, M. Spaliński, and V. Svensson, Hydrodynamization in kinetic theory: Transient modes and the gradient expansion, *Phys. Rev. D* **97**, 091503 (2018).
- [33] M. Strickland, J. Noronha, and G. Denicol, Anisotropic nonequilibrium hydrodynamic attractor, *Phys. Rev. D* **97**, 036020 (2018).
- [34] A. Behtash, C. N. Cruz-Camacho, and M. Martinez, Far-from-equilibrium attractors and nonlinear dynamical systems approach to the Gubser flow, *Phys. Rev. D* **97**, 044041 (2018).
- [35] P. Romatschke, Relativistic Fluid Dynamics Far From Local Equilibrium, *Phys. Rev. Lett.* **120**, 012301 (2018).
- [36] P. B. Arnold, G. D. Moore, and L. G. Yaffe, Transport coefficients in high temperature gauge theories. 2. Beyond leading log, *J. High Energy Phys.* **05** (2003) 051.
- [37] J. Rafelski and B. Muller, Strangeness Production in the Quark-Gluon Plasma, *Phys. Rev. Lett.* **48**, 1066 (1982); Erratum, *Phys. Rev. Lett.* **56**, 2334(E) (1986).
- [38] E. V. Shuryak, Two Stage Equilibration in High-Energy Heavy Ion Collisions, *Phys. Rev. Lett.* **68**, 3270 (1992).
- [39] D. Gelfand, F. Hebenstreit, and J. Berges, Early quark production and approach to chemical equilibrium, *Phys. Rev. D* **93**, 085001 (2016).
- [40] N. Tanji and J. Berges, Nonequilibrium quark production in the expanding QCD plasma, *Phys. Rev. D* **97**, 034013 (2018).
- [41] T. S. Biro, E. van Doorn, B. Muller, M. H. Thoma, and X. N. Wang, Parton equilibration in relativistic heavy ion collisions, *Phys. Rev. C* **48**, 1275 (1993).
- [42] D. M. Elliott and D. H. Rischke, Chemical equilibration of quarks and gluons at RHIC and LHC energies, *Nucl. Phys.* **A671**, 583 (2000).
- [43] K. Geiger and B. Muller, Dynamics of parton cascades in highly relativistic nuclear collisions, *Nucl. Phys.* **B369**, 600 (1992).
- [44] V. Borchers, J. Meyer, S. Gieseke, G. Martens, and C. C. Noack, A Poincare covariant parton cascade model for ultrarelativistic heavy ion reactions, *Phys. Rev. C* **62**, 064903 (2000).
- [45] Z. Xu and C. Greiner, Thermalization of gluons in ultrarelativistic heavy ion collisions by including three-body interactions in a parton cascade, *Phys. Rev. C* **71**, 064901 (2005).
- [46] J.-P. Blaizot, B. Wu, and L. Yan, Quark production, Bose-Einstein condensates and thermalization of the quark-gluon plasma, *Nucl. Phys.* **A930**, 139 (2014).
- [47] M. Ruggieri, S. Plumari, F. Scardina, and V. Greco, Quarks production in the quark-gluon plasma created in relativistic heavy ion collisions, *Nucl. Phys.* **A941**, 201 (2015).
- [48] P. B. Arnold, G. D. Moore, and L. G. Yaffe, Effective kinetic theory for high temperature gauge theories, *J. High Energy Phys.* **01** (2003) 030.
- [49] T. Lappi and L. McLerran, Some features of the glasma, *Nucl. Phys.* **A772**, 200 (2006).
- [50] F. Gelis, E. Iancu, J. Jalilian-Marian, and R. Venugopalan, The color glass condensate, *Annu. Rev. Nucl. Part. Sci.* **60**, 463 (2010).
- [51] T. Lappi, Gluon spectrum in the glasma from JIMWLK evolution, *Phys. Lett. B* **703**, 325 (2011).
- [52] E. Braaten and R. D. Pisarski, Soft amplitudes in hot gauge theories: A general analysis, *Nucl. Phys.* **B337**, 569 (1990).
- [53] L. D. Landau and I. Pomeranchuk, Electron cascade process at very high-energies, *Dokl. Akad. Nauk Ser. Fiz.* **92**, 735 (1953).
- [54] L. D. Landau and I. Pomeranchuk, Limits of applicability of the theory of bremsstrahlung electrons and pair production at high-energies, *Dokl. Akad. Nauk Ser. Fiz.* **92**, 535 (1953).

- [55] A. B. Migdal, Bremsstrahlung and pair production in condensed media at high-energies, *Phys. Rev.* **103**, 1811 (1956).
- [56] A. B. Migdal, Quantum kinetic equation for multiple scattering, *Dokl. Akad. Nauk Ser. Fiz.* **105**, 77 (1955).
- [57] Anisotropic systems suffer from the presence of unstable plasma modes [58–60], which could change the kinetic dynamics [61,62]. However, detailed 3 + 1D classical-statistical YM simulations found no effects of plasma instabilities beyond very early times [25,26]. Therefore, we will use isotropic approximations, which remove the unstable modes from the kinetic description. Note that there are no unstable fermionic modes [63,64].
- [58] S. Mrowczynski, Stream instabilities of the quark-gluon plasma, *Arles Multipart. Dyn.* **1988**, 0499; *Phys. Lett. B* **214**, 587 (1988); Erratum, *Phys. Lett. B* **656**, 273(E) (2007).
- [59] S. Mrowczynski, Plasma instability at the initial stage of ultrarelativistic heavy ion collisions, *Phys. Lett. B* **314**, 118 (1993).
- [60] S. Mrowczynski and M. H. Thoma, Hard loop approach to anisotropic systems, *Phys. Rev. D* **62**, 036011 (2000).
- [61] A. Kurkela and G. D. Moore, and B. Flow, Plasma instabilities, and thermalization, *J. High Energy Phys.* **11** (2011) 120.
- [62] A. Kurkela and G. D. Moore, Thermalization in weakly coupled nonabelian plasmas, *J. High Energy Phys.* **12** (2011) 044.
- [63] S. Mrowczynski, Quasiquarks in two stream system, *Phys. Rev. D* **65**, 117501 (2002).
- [64] B. Schenke and M. Strickland, Fermionic collective modes of an anisotropic quark-gluon plasma, *Phys. Rev. D* **74**, 065004 (2006).
- [65] A. Kurkela and A. Mazeliauskas, Chemical equilibration in weakly coupled QCD, *Phys. Rev. D* **99**, 054018 (2019).
- [66] J. D. Bjorken, Highly relativistic nucleus-nucleus collisions: The central rapidity region, *Phys. Rev. D* **27**, 140 (1983).
- [67] M. C. A. York, A. Kurkela, E. Lu, and G. D. Moore, UV cascade in classical Yang-Mills theory via kinetic theory, *Phys. Rev. D* **89**, 074036 (2014).
- [68] J. Ghiglieri, G. D. Moore, and D. Teaney, Jet-medium interactions at NLO in a weakly-coupled quark-gluon plasma, *J. High Energy Phys.* **03** (2016) 095.
- [69] D. Teaney (private communication).
- [70] P. Aurenche, F. Gelis, and H. Zaraket, A simple sum rule for the thermal gluon spectral function and applications, *J. High Energy Phys.* **05** (2002) 043.
- [71] A. Kurkela, A. Mazeliauskas, J.-F. Paquet, S. Schlichting, and D. Teaney, Effective kinetic description of event-by-event pre-equilibrium dynamics in high-energy heavy-ion collisions, [arXiv:1805.00961](https://arxiv.org/abs/1805.00961).
- [72] A. Kurkela, A. Mazeliauskas, J.-F. Paquet, S. Schlichting, and D. Teaney, Matching the non-equilibrium initial stage of heavy ion collisions to hydrodynamics with QCD kinetic theory, [arXiv:1805.01604](https://arxiv.org/abs/1805.01604).
- [73] M. Tanabashi *et al.* (Particle Data Group), Review of particle physics, *Phys. Rev. D* **98**, 030001 (2018).
- [74] J. Ghiglieri, G. D. Moore, and D. Teaney, QCD shear viscosity at (almost) NLO, *J. High Energy Phys.* **03** (2018) 179.
- [75] J. Ghiglieri, G. D. Moore, and D. Teaney, Second-Order Hydrodynamics in Next-to-Leading-Order QCD, *Phys. Rev. Lett.* **121**, 052302 (2018).
- [76] We determine  $\eta/s(\lambda)$  numerically from near-equilibrium pressure anisotropy evolution in longitudinally expanding system [65].
- [77] H. Kouno, M. Maruyama, F. Takagi, and K. Saito, Relativistic hydrodynamics of quark-gluon plasma and stability of scaling solutions, *Phys. Rev. D* **41**, 2903 (1990).
- [78] A. Muronga, Second Order Dissipative Fluid Dynamics for Ultrarelativistic Nuclear Collisions, *Phys. Rev. Lett.* **88**, 062302 (2002); *Phys. Rev. Lett.* Erratum **89**, 159901(E) (2002).
- [79] Note that the definition of  $\tau_{\text{hydro}}$  in Eq. (8) differs from the one used in Refs. [71,72].
- [80] C. Shen, Z. Qiu, H. Song, J. Bernhard, S. Bass, and U. Heinz, The iEBE-VISHNU code package for relativistic heavy-ion collisions, *Comput. Phys. Commun.* **199**, 61 (2016).
- [81] H. Niemi, K. J. Eskola, and R. Paatelainen, Event-by-event fluctuations in a perturbative QCD + saturation + hydrodynamics model: Determining QCD matter shear viscosity in ultrarelativistic heavy-ion collisions, *Phys. Rev. C* **93**, 024907 (2016).
- [82] A. Bazavov *et al.* (HotQCD Collaboration), Equation of state in (2 + 1)-flavor QCD, *Phys. Rev. D* **90**, 094503 (2014).
- [83] S. Borsanyi *et al.*, Calculation of the axion mass based on high-temperature lattice quantum chromodynamics, *Nature (London)* **539**, 69 (2016).
- [84] J. E. Bernhard, J. S. Moreland, S. A. Bass, J. Liu, and U. Heinz, Applying Bayesian parameter estimation to relativistic heavy-ion collisions: simultaneous characterization of the initial state and quark-gluon plasma medium, *Phys. Rev. C* **94**, 024907 (2016).
- [85] For more accurate description, extensions of our study including transverse expansion are needed [86].
- [86] A. Kurkela, U. A. Wiedemann, and B. Wu, Kinetic transport is needed to reliably extract shear viscosity from pA and AA data, [arXiv:1805.04081](https://arxiv.org/abs/1805.04081).
- [87] B. Muller and K. Rajagopal, From entropy and jet quenching to deconfinement?, *Eur. Phys. J. C* **43**, 15 (2005).
- [88] P. Hanus, Entropy in Pb-Pb collisions at the LHC, Bachelor's thesis, University of Heidelberg, 2018.
- [89] Note that the combination  $(\tau/\tau_R)^3(\tau/R)^{-2}$  is independent of time.
- [90] For example, our model neglects quark masses, which could delay flavor equilibration. Even then the relation of strangeness content in the QGP and hadronic phase is not trivial [91–93].
- [91] K. S. Lee, M. J. Rhoades-Brown, and U. W. Heinz, Quark-gluon plasma versus hadron gas: What can we learn from hadron abundances?, *Phys. Rev. C* **37**, 1452 (1988).
- [92] J. Sollfrank and U. W. Heinz, The role of strangeness in ultrarelativistic nuclear collisions, *Quark-Gluon Plasma 2*, 555 (1995).
- [93] J. Letessier, A. Tounsi, U. W. Heinz, J. Sollfrank, and J. Rafelski, Strangeness conservation in hot nuclear fireballs, *Phys. Rev. D* **51**, 3408 (1995).
- [94] Z. Citron *et al.*, Future physics opportunities for high-density QCD at the LHC with heavy-ion and proton beams, in *HL/HE-LHC Workshop: Workshop on the Physics of HL-LHC, and Perspectives at HE-LHC* (Geneva, Switzerland, 2018).